Applied Catalysis B: Environmental 237 (2018) 214–227

Contents lists available at ScienceDirect

Applied Catalysis B: Environmental

journal homepage: www.elsevier.com/locate/apcatb

Alkali and earth alkali modified CuO_x/SiO_2 catalysts for propylene partial oxidation: What determines the selectivity?

Janvit Teržan[a,b], Petar Djinović[a,*], Janez Zavašnik[c,d], Iztok Arčon[b,e], Gregor Žerjav[a], Matjaž Spreitzer[b,f], Albin Pintar[a]

[a] Department for Environmental Sciences and Engineering, National Institute of Chemistry, Hajdrihova 19, SI-1001 Ljubljana, Slovenia
[b] Jožef Stefan International Postgraduate School, Jamova cesta 39, SI-1000 Ljubljana, Slovenia
[c] Centre for Electron Microscopy and Microanalysis, Jožef Stefan Institute, Jamova cesta 39, 1000 Ljubljana, Slovenia
[d] Max-Planck-Institut für Eisenforschung GmbH, Max-Planck-Straße 1, 40237 Düsseldorf, Germany
[e] University of Nova Gorica Vipavska cesta 13, Nova Gorica, 5000, Slovenia
[f] Advanced Materials Department, Jožef Stefan Institute, Jamova cesta 39, 1000 Ljubljana, Slovenia

ARTICLE INFO

Keywords:
Propylene
Acrolein
Selective oxidation
Epoxidation
Alkali doping
Nucleophilic oxygen

ABSTRACT

In this work, CuO_x/SiO_2 catalysts were investigated in the propylene partial oxidation reaction. Ordered mesoporous silica (KIT-6) was used to deposit 1–10 wt. % copper and subsequently modified with Na, K and Ca. The synthesized materials were characterized by N_2 physisorption, XRD, TEM-EDS, CO_2-TPD, *operando* UV/Vis DRS, *operando* XANES and pyridine DRIFT spectroscopy. Regardless of the CuO_x loading, catalyst deactivation was observed during propylene oxidation reaction in non-modified catalysts, which was related to sintering of oligomeric $[Cu\text{-}O\text{-}Cu]_n$ species. Sintering of CuO_x is strongly promoted under a reducing propylene atmosphere and related to the presence of Cu^{+1}. The resulting bulk CuO_x promotes acrolein selectivity. We produced modified catalysts with finely dispersed alkali metal cations, associated with the subnanometer CuO_x phase, resulting in a greatly stabilized morphology and catalytic activity. *Operando* XANES analysis revealed that a substantial fraction of Cu^{2+} is transformed to Cu^{+} during the propylene oxidation reaction (52–68%, depending on the modifying atom). Also, the dynamics of reaching the quasi steady oxidation state differ strongly. The kinetics of oxygen abstraction and replenishment are substantially different, indicative of modified chemistry of the nucleophilic oxygen species, present in 5CuNa catalyst in contrast to others (5Cu and 5CuCa). We propose that Cu^{+} is not crucial for PO formation. Instead the electropositive Na^{+} and K^{+} decrease the nucleophilic strength of oxygen in CuO_x, by attracting its electrons. Consequently, the catalytic action of oxygen changes from oxidative attack on the allylic hydrogen to oxygen insertion into the C=C bond of propylene. This results in a noticeable selectivity shift from acrolein to propylene oxide. The effect of calcium on decreasing the nucleophilic character of O species in CuO_x is negated by charge compensation by strongly adsorbed hydroxyl groups and Ca modification for PO selectivity is inefficient. Additionally we found, that further oxidation of propylene oxide is, most likely, the main factor determining high selectivity for CO_x products. The alkali modification which increases the PO selectivity does not function via elimination of LAS, but exclusively through attenuation of nucleophilic character of oxygen species.

1. Introduction

Propylene can be catalytically converted into several useful C_3 oxygenates, such as propylene oxide (PO), propanal and acrolein [1]. Propylene oxide is a highly desired chemical as it is used in the production of propylene glycol ethers, propylene glycol and polyether polyols [2]. Most PO is produced by the mature and industrially established chlorohydrin process (CHPO), PO/styrene and PO/tert-butyl processes through a peroxidized intermediate and lately the hydrogen peroxide to propylene oxide (HPPO) process over single-site TS-1 or Ti-MWW catalysts using H_2O_2 as an oxidant. HPPO process uses H_2O_2 as the oxidant and produces PO with a selectivity of 99% [3]. There are several drawbacks for each of these processes, such as high cost of the reactants (H_2O_2), large quantity and a low price of the co-products (styrene monomer or tert-butyl alcohol) and environmental pollution (chlorinated lime as side product) [2,4].

The above mentioned drawbacks have driven research into direct gas-phase epoxidation of propylene using molecular oxygen. The

* Corresponding author.
E-mail address: petar.djinovic@ki.si (P. Djinović).

https://doi.org/10.1016/j.apcatb.2018.05.092
Received 4 April 2018; Received in revised form 28 May 2018; Accepted 30 May 2018
Available online 31 May 2018
0926-3373/ © 2018 Elsevier B.V. All rights reserved.

reaction suffers from conversion vs. selectivity issue: at low conversions (~1%), high PO selectivities can be achieved (~77%), whereas at higher conversions (above 15%), low PO selectivities (below 40%) are obtained [4]. By using a gas mixture of H_2 and O_2 as the oxidant over Au/TS-1 or Ti doped amorphous silica catalyst, PO selectivity above 90% can be achieved, but the conversions are very low (below 1%) [5]. With titanium-containing catalysts, deactivation is a persistent problem and is related to irreversible binding of reaction intermediates to the active sites, forming stable bidentate species [6,7].

Considerable amount of research has been performed on silver based catalyst, as silver is a very efficient ethylene epoxidation catalyst [4]. The issue with silver is that it is a very strong oxidant of the allylic hydrogen (which is not present in ethylene), resulting in PO selectivity during propylene epoxidation being substantially shifted towards total combustion [8,9]. For example, Lu et al. [9] performed propylene epoxidation over Ag catalysts immobilized on several supports (MgO, $CaCO_3$, CeO_2, …) and observed that CO_2 and H_2O were the main reaction products with the highest PO selectivity of 5.4%.

Regardless of the oxidant and metal used for propylene epoxidation, several studies have shown that an oxametallacycle (OMMC) is the necessary intermediate [10–12]. DFT calculations of the OMMC stability on several transition metals (Me) have shown that the metal plays a significant role. It was also predicted that for achieving high PO selectivity, the relative stability of the OMMC (desorption enthalpy) should be similar to the relative heat of PO adsorption on the same surfaces [10]. In a study of ethylene epoxidation, Kokalj et al. [11] also showed that specific bond strengths (Me-C vs. Me-O) and consequently order of their cleavage during OMMC desorption has a critical impact on selectivity. Their calculations showed that in case when Me-O bond cleaves first, acetaldehyde is produced, whereas initial cleavage of the Me-C bond results in ethylene oxide as the preferred product.

Copper catalysts also received a fair share of attention in regards to propylene epoxidation and oxametallacycle formation [1,8,13–16]. Torres et al. [1] studied the ability of Ag and Cu to oxidize the allylic hydrogen and form an oxametallacycle. Their studies were aimed at a metal catalyst (modelled as a perfect slab), and showed that copper, in contrast to silver, favours oxymetallacycle formation and not allylic hydrogen striping. They also calculated that the surface bound oxygen species on copper are less basic (less nucleophilic) than the ones bound on silver, indicating their lower tendency to react with allylic hydrogen. DFT studies performed by Yang et al. [12] have shown that copper in +1 oxidation state is preferred for oxametallacycle formation, as compared to Cu° or Cu^{2+}. Realistically, the oxidation state of copper during propylene epoxidation is either +1 or +2 as was shown by Greiner et al. [15] and Monneier et al. [8,16]. Further, Marimuthu et al. [17] varied the copper oxidation state in Cu/SiO_2 catalysts by illumination and observed that metallic copper is formed upon illumination which favours PO formation, whereas CO_2 and acrolein are produced over Cu^{1+} in dark.

Hua et al [18]. identified that the propylene epoxidation reaction occurs via the Mars-van Krevelen mechanism on Cu_2O. They studied different crystal planes of Cu_2O and how the coordination of the terminating lattice oxygen influences selectivity of the reaction. They found that one coordinated Cu^{1+} on Cu_2O [111] crystalline plane produces predominantly acrolein, two- coordinated oxygen on Cu_2O [100] crystalline plane produces CO_2, whereas three-coordinated oxygen on Cu_2O [110] crystalline plane predominantly produces PO.

The main drawback preventing high PO selectivity during direct gas-phase propylene epoxidation with molecular oxygen are the unfavourable properties of the allylic hydrogen (more acidic as compared to vinylic hydrogen) and strong Brønsted basicity of CuO_x lattice oxygen species (O^{2-}). To favour PO selectivity, nature of the oxygen species needs to be modulated, namely their Brønsted basicity (nucleophilicity) needs to be lowered. One way to modulate their basic character is with alkali (Na, K, Rb, Cs) or earth alkali (Be, Mg, Ca) modifications [13,19–22]. Wang et al. [19] investigated CuO_x/SBA-15 catalysts and noticed the highest PO selectivity when using K (~5% conversion, ~27% PO selectivity) or Na modification (~7% conversion, ~9% PO selectivity). The same study also reports that addition of earth alkali metals (Mg, Ca, Ba) leads to negligible PO selectivities (< 1%) and higher catalytic activity as compared to non-doped catalysts.

In this work, we investigated the effect of Na, K and Ca modification of highly dispersed CuO_x species on KIT-6 silica catalysts during direct gas-phase propylene oxidation. Relevant *ex-situ*, *in-situ* and *operando* techniques were applied to the synthesized materials revealing the pivotal role of CuO_x morphology and nature of the oxygen species in governing catalytic stability and PO selectivity.

2. Experimental

2.1. Catalyst preparation

2.1.1. Synthesis of KIT-6 silica

The KIT-6 silica support material was synthesized according to a procedure from Kim et al. [23]. For a typical 5 g batch of support, 8.1 g of Pluronic P123 (Sigma-Aldrich) was dissolved in a mixture consisting of 15.9 g of HCl (35 wt. %) and 292.2 g of deionized water. To accelerate P123 dissolution, the mixture was ultrasonicated for 15 min without heating. After complete dissolution, 8.1 g of butanol was added and additionally ultrasonicated for 15 min. The mixture was stirred at 35 °C for 5 h before 17.4 g of tetraethoxysilane (TEOS, Sigma-Aldrich) was added. The solution was left to stir for 24 h at 35 °C and afterwards transferred to a Teflon lined stainless steel autoclave for an additional 24 h at 130 °C. The white precipitate was collected and washed by centrifugation (9000 rpm, 90 s) until no more Cl^- was detected in the supernatant, dried overnight at 50 °C and calcined at 550 °C (1 °C min^{-1} to 550 °C, isothermal for 5 h).

2.1.2. Deposition of CuO_x phase over the KIT-6 silica support

Copper CuO_x/SiO_2 catalysts were prepared by precipitation of the copper-ammonia complex via dilution hydrolysis method (inspired by Meng et al. [24]). Different amounts of $Cu(NO_3)_2 \times 3H_2O$ (95, 190 and 380 mg), corresponding to the nominal copper content of 2.5, 5 and 10 wt. %, were dissolved in 40 mL of deionized water. After dissolution, 1 g of KIT-6 was added and stirred for 15 min. The pH value of the solution was adjusted to 9.0 with 27% ammonia solution and left stirring for 3 h. To induce the hydrolysis of the copper-ammonia complex, the suspension was diluted with 150 mL of deionized water added dropwise over the course of 2.5 h. The impregnated support was separated from the supernatant by centrifugation (9000 rpm, 90 s), dried for 5 h at 80 °C and calcined at 350 °C (2 °C min^{-1} to 350 °C, isothermal for 3 h).

The samples were denoted as xCu, where x represents the nominal content (wt. %) of copper on the silica support. The actual copper content in the synthesized materials was estimated using a photometric copper test Spectroquant® (Merck) on the supernatant solution after centrifugation. In all cases 90–100 % deposition of copper in the prepared CuO_x/SiO_2 catalysts was confirmed. Quantitative analysis of Cu, Na, K and Ca content was performed with the energy-dispersive X-ray detector (FE-SEM SUPRA 35 V P, Carl Zeiss, Inca 400, Oxford Instruments).

2.1.3. Alkali and earth alkali modification of the CuO_x/SiO_2 catalysts

For the alkali and earth alkali modification, 30 mL of aqueous solutions of nitrate salts (0.1 M $NaNO_3$, 0.05 M $Ca(NO_3)_2$ and 0.1 M KNO_3) was used. After complete dissolution of the salt, 300 mg of the CuO_x/SiO_2 catalyst was added to the solution. The suspension was stirred for 3 h. The modified catalyst was separated from the supernatant by centrifugation (9000 rpm, 90 s), dried for 5 h at 80 °C and calcined at 350 °C (2 °C min^{-1} to 350 °C, isothermal for 3 h).

The samples were denoted as xCuy, where x represent the copper

content and y the dopant (*e.g.* 5CuNa stands for a 5 wt. % CuO_x/SiO_2 catalyst modified with sodium).

2.2. Characterization and catalytic testing

2.2.1. BET specific surface area and porosity

The BET surface area, total pore volume and average pore size distribution were determined from N_2 adsorption/desorption isotherms obtained at −196 °C (Micromeritics, model TriStar II 3020). Prior to analysis, the samples were degassed in N_2 stream (purity 6.0 by Linde), using a SmartPrep degasser (Micromeritics) at 90 °C for 60 min, and followed for 120 min at 180 °C. Pore size distribution curves and total pore volume were calculated by the BJH (Barrett-Joyner-Halenda) method from the desorption branch of the isotherm. Micropore contribution was evaluated with the t-plot method.

2.2.2. X-ray diffraction

Mesoporous ordering of the prepared CuO_x/SiO_2 catalysts was analyzed using powder X-ray diffraction (XRD) analysis. The PANalytical Empyrean diffractometer using in Bragg-Brentano geometry and Cu Kα radiation was used. XRD patterns were recorded in the 2θ range from 0.5° to 3°, with a measurement step of 0.0131° and a step time of 500 s. The same conditions were also used for identification of crystalline phases, for which the 10Cu catalyst was scanned in the 2θ range from 10° to 60°.

2.2.3. Transmission electron microscopy

For TEM analyses samples were first dispersed in absolute ethanol and sonicated to prevent agglomeration; such prepared suspension was transferred onto commercial lacey-carbon Ni or Au support grids. Due to the nature of the analyses a double-tilting analytical Be holder was used. The core morphology of the samples was studied by Schottky field-emission transmission electron microscope (JEM-2200FS, JEOL Ltd.), operating at 200 kV. The chemistry of the samples was analysed in scanning-TEM mode using windowless ultrafast large angle 100 mm^2 SDD-EDS spectrometer (EX-24200M1G2T, JEOL), allowing efficient collection of X-rays. High-angle annular dark field (HAADF) detector (EM-24630UHADF, JEOL) was used for collecting of only incoherently scattered electrons, highly sensitive to variations in the atomic number (Z contrast).

Due to the beam sensitivity of SiO_2 mesoporous materials under the electron beam, various approaches have been employed to achieve reliable results. Although a low operating voltage (e.g. 80 kV) is generally considered to avoid severe electron beam induced knock-on damage, we choose to limit the primary electron beam with smallest condenser aperture, in attempt to obtain a sufficiently high current in the small probe used for chemical analysis. This resulted in improved signal-to-background and signal-to-noise ratios, and due to short acquisition time also in reduced beam damage and enhanced detectability. Additionally, a hard X-ray aperture was used to limit the amount of scattered electrons and X-rays to speed up the EDS counting and hence analysis time.

2.2.4. UV/Vis diffuse reflectance measurements

Structural and electronic properties of CuO_x phase with and without alkali modification were analyzed with UV/Vis spectrophotometry (Perkin Elmer, model Lambda 35) at room temperature in the range between 200 and 1100 nm. The powder samples were analyzed using the RSA-PE-19 M Praying Mantis accessory with Spectralon© as the background standard. *Operando* UV/Vis diffuse reflectance (DR) measurements were performed in order to obtain insights into the working state of the catalyst during the epoxidation reaction, as well as reversibility of redox and morphological changes. The experiments were performed in the HVC-VUV Praying Mantis Reaction Chamber (Harrick) using the Perkin Elmer Lambda 650 UV/Vis spectrophotometer. Spectra were recorded over catalyst samples exposed to pre-treatment in 20% O_2/He at 350 °C for 30 min, followed by 100 min of oxidation reaction (16.7% C_3H_6, 16.7% O_2 and 66.7% of He at 350 °C). Afterwards, the catalysts were regenerated in 20% O_2/He at 350 °C for 30 min, followed by exposure to pure C_3H_6. Finally, the catalysts were re-oxidized for 115 min in 20% O_2/He at 350 °C. The analytical protocol is schematically shown in Supplementary Information (Fig. S1).

2.2.5. Acid site probing using DRIFT spectroscopy

Lewis and Brønsted acidity of the prepared catalysts was investigated using pyridine as the probe molecule. Experiments were performed in a DiffusIR cell (PIKE Technologies) attached to a Perkin Elmer Frontier spectrometer. The powdered samples (10 mg) were pretreated at 350 °C for 20 min in a flow of N_2. After cooling to 25 °C, the samples were saturated with pyridine vapour/N_2 gas stream for 10 min and subsequently evacuated for 60 min at 10^{-5} mbar (Pfeiffer Vacuum turbomolecular pump, model HiCube). The spectra collected are the average of 32 scans with a resolution of 4 cm^{-1}.

2.2.6. Temperature programmed desorption (TPD) of CO_2

Basicity of the prepared catalysts was analyzed using CO_2 as the probe molecule. Experiments were performed in a Micromeritics AutoChem II 2920 apparatus. The sample (100 mg) was positioned inside a U-shaped quartz reactor and pre-treated in a flow 5% O_2/He at 350 °C for 30 min. After pre-treatment, it was cooled to 0 °C and saturated with pure CO_2 (purity 5.3, Linde) for 30 min. Weakly adsorbed CO_2 was removed in a flow of pure He for 30 min. The samples were heated to 900 °C at 5 °C/min and CO_2 desorption was monitored by a mass spectrometer (Pfeiffer Vacuum, model ThermoStar™ GSD320) following the characteristic $m/z = 44$ fragment. Pulses of 0.5 mL CO_2 were used as an external standard for CO_2-TPD signal calibration.

Additional information on the nature of desorbed CO_2 was obtained by DRIFT analysis (Perkin Elmer Frontier spectrometer equipped with a DiffuseIR cell). During the experiment, 10 mg of catalyst was pretreated in a flow 5% O_2/He at 350 °C for 30 min. After pre-treatment the sample was cooled to 0 °C and saturated with 50% CO_2/He for 30 min, followed by degassing in pure He for 60 min, and gradual heating to 900 °C with a ramp of 10 °C/min. DRIFT spectra were recorded in the relevant temperature intervals, revealing the nature of desorbed CO_2 (Fig. S2).

2.2.7. Operando Cu K-edge XANES

The Cu K-edge X-ray absorption spectra (XAS) of 5Cu, 5CuNa and 5CuCa catalysts were recorded *in-situ* during the propylene oxidation reaction at 350 °C in transmission detection mode at the XAFS beamline of the ELETTRA synchrotron radiation facility in Trieste, Italy. The catalyst samples were prepared in the form of homogeneous pellets, pressed from micronized sample powder mixed with BN powder, with the total absorption thickness (μd) of about 2.5 above the investigated Cu K-edge. Pellets were inserted in a tubular oven reactor (Carbolite MTF 12/25/400) with 20 μm aluminum foil windows, filled with a gas mixture composed of 80% He and 20% O_2 at 1 bar. The XAS spectra were measured *in-situ*: (i) at room temperature, (ii) at 350 °C in the He/O_2 atmosphere and (iii) during the catalytic propylene oxidation reaction at 350 °C in a C_3H_6/O_2/He stream (16.7% C_3H_6, 16.7% O_2, 66.6% He, total flowrate of 30 ml/min). After propylene addition, the samples were measured repeatedly until the quasi-equilibrium state in the catalyst was reached (up to 10 XAS spectra were collected per sample). Details of the XAS measurements and apparatus settings are provided in the supplementary information file.

2.3. Catalytic tests

Catalytic performance of the synthesized catalysts was tested in a tubular fixed-bed quartz reactor (I.D. = 10 mm) at atmospheric pressure. In a typical experiment, 50 mg of the catalyst was diluted with 200 mg of SiC and fixed between two quartz wool flocks. Before the catalytic tests, the samples were pre-treated in a flow of O_2 and He (5

and 20 mL/min, respectively) at 350 °C. After 20 min of pre-treatment, propylene (Messer, purity 2.5) at 5 mL/min was added to the gas mixture. The reaction products were monitored by gas chromatography (Agilent, model 7890 A); the GC device was equipped with the DB-WAXETR (Agilent) and the HP-PlotQ columns and a TCD detector. Blank experiment confirmed no propylene conversion occurring at 350 °C in absence of the catalyst.

The conversion of propylene was calculated using Eq. (1), where n_{C3H6i} and n_{C3H6O} are moles of propylene at the inlet and outlet of the reactor.

$$\%_{conversion} = \frac{(n_{C_3H_6\,i} - n_{C_3H_6\,o})}{n_{C_3H_6\,i}} \times 100\,\% \quad (1)$$

Reaction product selectivities were calculated according to Eq. (2), where n_i are moles of product i and n_{C3H6C} are moles of propylene converted.

$$\%_{selectivity} = \frac{n_i}{n_{C_3H_6\,c}} \times 100\,\% \quad (2)$$

3. Results and discussion

3.1. Characterization of catalysts

3.1.1. Specific surface area and pore size/volume

The N_2 adsorption/desorption isotherms of the KIT-6 support and all CuO_x/SiO_2 catalysts are of type IV with a sharp capillary condensation step and H1 hysteresis loop, indicative of large channel-like pores (Fig. 1a). Pore size distribution in the synthesized support is in the range of 7–10 nm (Fig. 1b) with negligible contribution of larger pores originating from inter-particle porosity.

After CuO_x deposition, a decrease of about 25% in BET specific surface area and pore volume occurs, as compared to pure KIT-6 silica support (Table 1). Also, pore size distribution shifts towards lower values (Fig. 1b), suggesting that CuO_x phase lies inside the pores of the silica support. Subsequent modification of the CuO_x catalysts with sodium induced only slight changes in surface area, pore diameter and pore volume. The micropore volume and micropore surface area represent a small fraction of the total pore volume and available specific surface area in the synthesized catalysts (less than 2 and 8%, respectively, Table 1).

3.1.2. X-ray diffraction examination

X-ray diffraction patterns at low 2θ angles of pure KIT-6 silica support, 5Cu, 10Cu and 10CuNa catalysts are illustrated in Fig. 2. All patterns show two peaks at approximately 2θ = 0.83 and 1.03° corresponding to the (211) and (220) reflections of the *Ia3d* cubic structure [25]. This indicates a well-ordered mesoporous structure of the KIT-6 support, which is maintained during subsequent copper and sodium modifications.

XRD analysis at higher 2θ angles was performed for the 10Cu catalyst (containing the highest Cu content) in order to identify possible crystalline phases present (Fig. S3). A broad diffraction peak in the 2θ range from 15° to 30° was observed, characteristic for amorphous silica. However, no diffraction peaks at 2θ values characteristic for CuO (2θ = 35.5 and 38.7°) or Cu_2O (2θ = 36.4 and 42.3°) can be seen, indicating a negligible fraction of CuO_x is present as bulk crystalline CuO in this catalyst. Same is expected for catalysts with a lower copper content.

3.1.3. TEM-EDS analysis

The BF-TEM micrographs of the pure silica support and 5CuNa sample revealed ordered mesoporous support structure (Fig. 3a), confirming results of XRD and N_2 physisorption analyses. HAADF-STEM imaging was used to visualize the CuO_x phase using Z contrast. The majority of visible CuO_x is present in form of small particles with a mean diameter of 4 nm (brighter spots, inset Fig. 3b). In addition, larger CuO_x clusters of 10–20 nm, concentrated in aggregates of 100–200 nm were also observed in the 5CuNa catalyst (Fig. 3c). With increasing copper loading (10CuNa catalyst), larger CuO_x aggregates (10–20 nm) become more abundant (Fig. 3d). STEM-EDS maps were performed, since they scan the sample without stopping the probe and therefore reduce electron beam damage to the sample. The elemental mapping (Fig. 3e) indicates that in addition to above mentioned CuO_x morphologies, highly dispersed (subnanometer) copper species densely covering the SiO_2 support are also present in the 5CuNa catalyst. Also, the elemental maps of sodium and copper overlap, suggesting the alkali dopant is closely associated with CuO_x phase (Fig. 3f).

3.1.4. UV/VIS DR analysis

Diffuse reflectance UV/Vis analysis of alkali modified and non-modified CuO_x/SiO_2 catalysts was performed to obtain additional insights into the structure of CuO_x moieties. The spectra show three distinct features (Fig. 4). The first peak stretching from 250 to approximately 320 nm is characteristic for charge transfer between mononuclear Cu^{2+} and oxygen [26].

The band at approximately 370–500 nm which increases in intensity with copper loading is characteristic of $[Cu–O–Cu]_n$-type (oligomeric

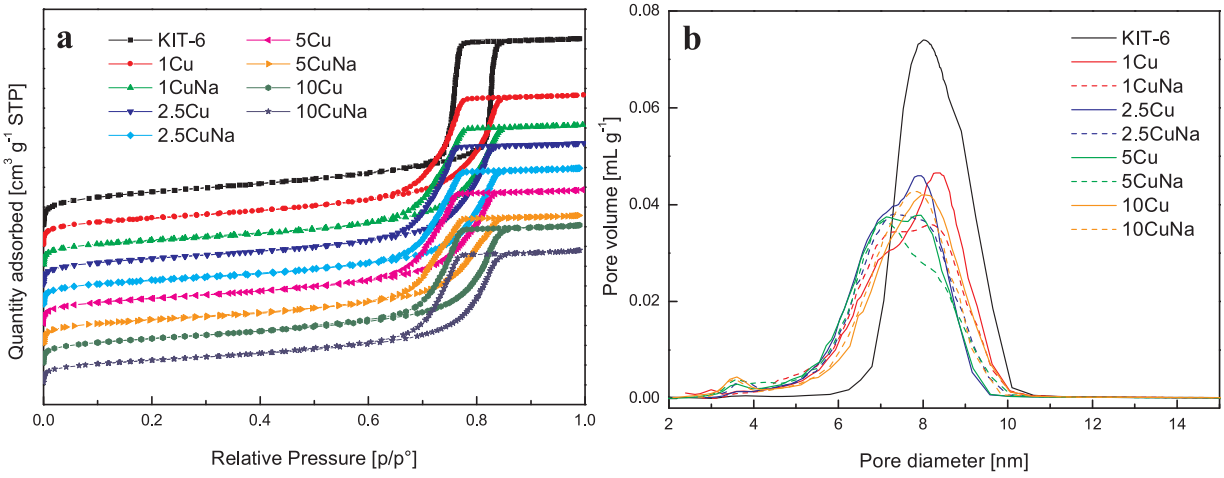

Fig. 1. a) N_2 adsorption/desorption isotherms of KIT-6 silica support and CuO_x/SiO_2 catalysts containing 1–10 wt. % Cu with and without Na modification. The isotherms are offset by 100 cm^3 N_2 g^{-1} STP for easier visualization.; b) Pore size distribution of pure KIT-6 SiO_2 support and CuO_x/SiO_2 catalysts with different copper loadings before and after Na modification.

Table 1
Material properties measured with N_2 physisorption technique.

	BET $m^2 \times g^{-1}$	Average pore diameter[a] nm	Total pore volume[a] $cm^3 \times g^{-1}$	Micropore volume[b] $cm^3 \times g^{-1}$	Micropore area[b] $m^2 \times g^{-1}$	External surface area[b] $m^2 \times g^{-1}$
KIT-6	615	8.3	1.48	0.023	49	566
1Cu	507	7.3	1.19	0.019	41	466
1CuNa	471	7.3	1.11	0.008	21	450
2.5Cu	490	7.1	1.12	0.015	35	455
2.5CuNa	462	7.1	1.09	0.009	21	441
5Cu	485	7.0	1.07	0.013	31	454
5CuNa	465	7.0	1.02	0.006	18	447
5CuK	378	7.0	1.04	0.010	28	350
5CuCa	404	7.0	1.03	0.011	32	372
10Cu	475	7.4	1.1	0.013	31	444
10CuNa	439	7.2	1.06	0.014	32	407

[a] Calculated using the BJH method.
[b] Calculated using the t-plot method.

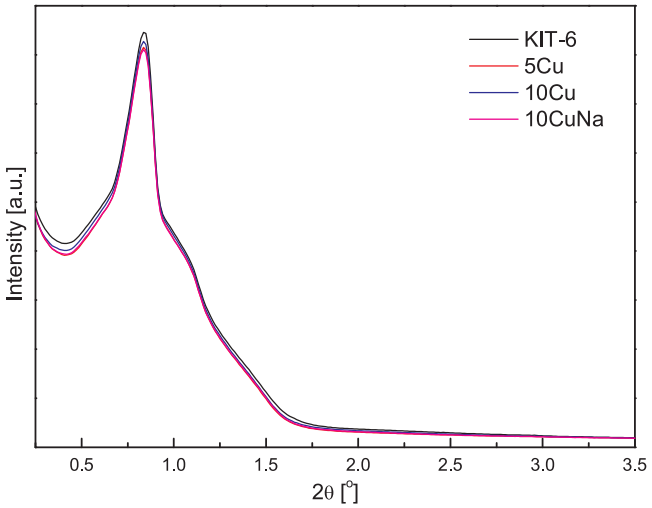

Fig. 2. X-ray diffraction patterns at low 2θ angles of pure KIT-6 silica support, 5Cu, 10Cu and 10CuNa catalysts.

species), which are different from bulk CuO and indicates progressive clustering of [Cu–O–Cu] moieties when increasing copper content from 2.5 to 10 wt. %. The broad but less intense band between 600–800 nm corresponds to the d-d transition of Cu^{2+} ions in an octahedral environment, which can be attributed to bulk CuO. Based on the dissimilarity in the UV/Vis DR spectra of bulk CuO (crystalline monoclinic CuO, red line in Fig. 4) and 10Cu catalyst (containing the highest copper loading), the bulk CuO species in octahedral coordination in this catalyst are not abundant and strongly distorted (possibly amorphous, which is in line with XRD results, Fig. S3) [19,27,28].

Catalysts modified with Na show a red shift of the shoulder at 370 nm, indicating oligomerization of the $[Cu–O–Cu]_n$ species, which was induced by the second calcination procedure applied after Na addition (Section 2.1.3). The same behaviour was observed with similar catalysts by Garcia-Aguilar et al. [22].

Thermal stability of the CuO_x species in presence of different alkali or earth alkali modifiers was tested by applying an additional calcination procedure to the 2.5Cu and 5Cu sample to equal the thermal history of 5CuNa, 5CuK or 5CuCa catalysts (Fig. 5).

A notable absorption red-shift was observed after the second calcination protocol for the 2.5Cu and 5Cu catalyst (black and magenta lines in Fig. 5) along with the increase of band intensity (centred at 700 nm) related to bulk CuO. These changes were much larger compared to modified catalysts (5CuNa ≈ 5CuK > 5CuCa) and show that alkali and earth alkali modifications strongly hinder sintering and oligomerization of the [Cu–O–Cu] species in oxidative atmosphere. Furthermore, a positive role of alkali modification is known, as He et al. [29] observed that Cs modification of CuO_x/SiO_2 catalysts resulted in a substantial decrease of the average CuO scattering domain size, suggesting re-dispersion of CuO phase.

3.1.5. *Operando* UV/Vis DRS analysis

The 5Cu and 5CuNa catalysts were analyzed to obtain relevant information on the structural and redox changes occurring under oxidative, reductive and realistic propylene oxidation conditions in the presence or absence of alkali dopant (Fig. 6). The analytical protocol is depicted in Fig. S1.

Spectra measured during the propylene oxidation reaction over 5Cu catalyst (16.7% C_3H_6, 16.7% O_2 and 66.6% of He, Fig. 6a) show the band between 250–370 nm, which is attributed to mononuclear Cu^{2+} and finely dispersed [Cu-O-Cu] moieties, and changes very little during the 100 min of reaction (Fig. 6a). Simultaneously, the band increases between 370–650 nm, indicating clustering of [Cu-O-Cu] oligomeric species and formation of larger CuO_x clusters.

The changes of the band between 250–370 nm in the 5CuNa catalyst during the propylene oxidation reaction are negligible (Fig. 6b). This indicates improved stability of mononuclear and oligomeric [Cu-O-Cu] moieties after Na modification. Simultaneously, the band between 370–650 nm increases (to a smaller extent compared to 5Cu catalyst) with reaction time.

Switching back to an oxidative atmosphere (16.7% C_3H_6, 16.7% O_2 and 66.6% of He → 20% O_2/He, (Fig. 6c and d) shows no change in the spectra of the 5Cu and 5CuNa catalysts, even after 30 min. Presence of Cu^{1+} was confirmed by *operando* XANES (described in detail in Section 3.1.8), which was independently observed during propylene epoxidation over a Cs^+ modified CuO_x/SiO_2 catalyst [29].

Switching to a purely reductive atmosphere (20% O_2/He → C_3H_6) results in a progressive increase of light absorption in the whole range of wavelengths (200–1100 nm) for both 5Cu and especially 5CuNa catalysts (Fig. 6e and f). This suggests the onset of substantial structural (distortion of CuO_x species due to oxygen elimination [28]) and redox changes, which occur in the same range of wavelengths. Metallic copper absorbs light in the range between 225–590 nm [28], whereas Cu_2O at wavelengths between 300 and 500 nm [30].

Returning to an oxidative atmosphere after reduction in propylene (C_3H_6 → 20% O_2/He, Fig. 6g and h) causes re-oxidation of the catalyst. Structural changes based on the evolution of the UV/Vis DR spectra suggest formation of bulk CuO and clustering of [Cu-O-Cu] oligomeric species. The structural changes of CuO_x induced by the redox cycle are, to a greater extent, reversible in the 5CuNa catalyst (spectrum returns closer to the value before the reduction). This suggests that Na modification acts as a sintering barrier preventing surface migration of copper species.

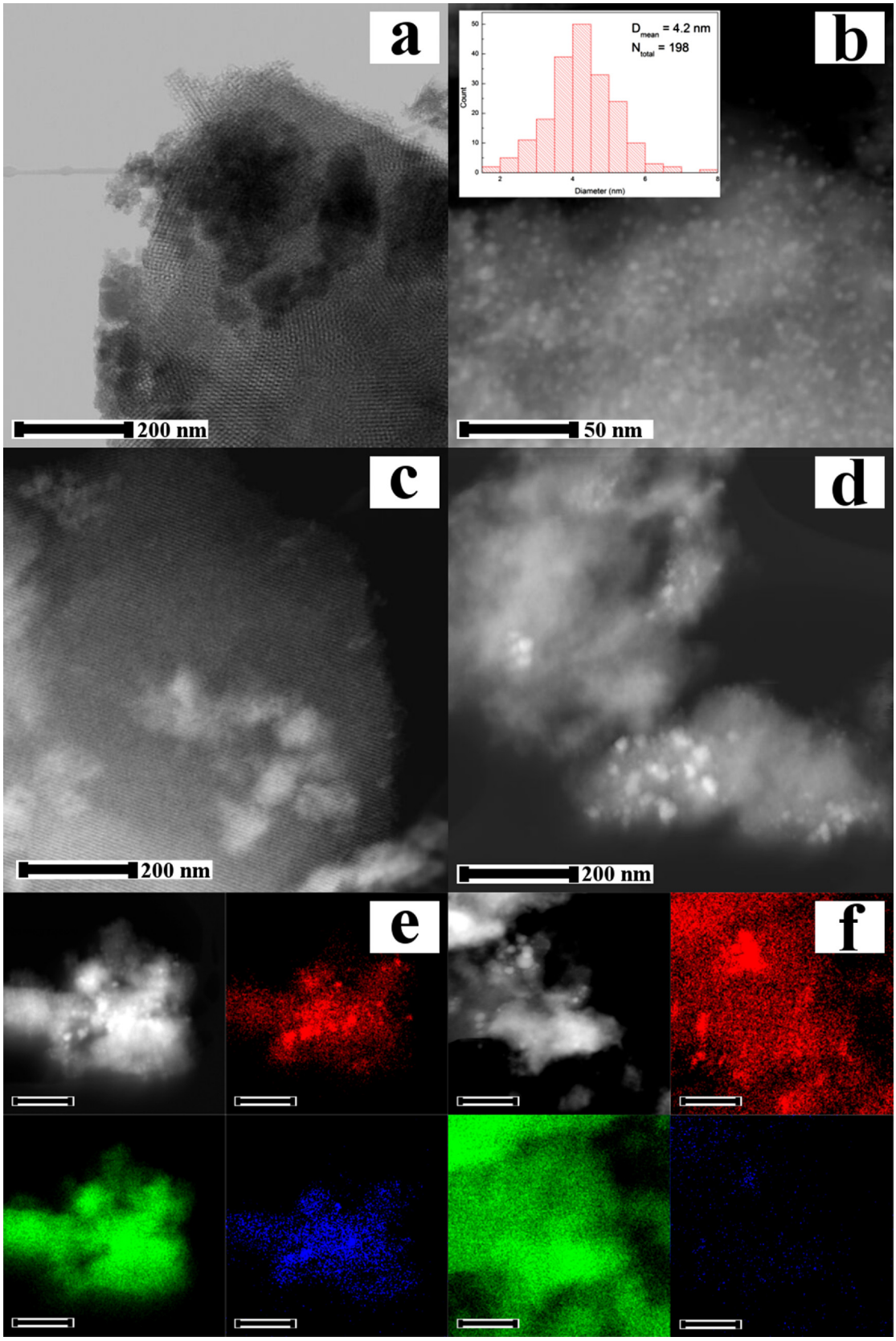

Fig. 3. a) BF-STEM image of the 5CuNa catalyst showing ordered mesoporous SiO_2 support, preserved also after Cu and Na modification, b) HAADF-STEM image of the 5CuNa catalyst with size distribution of CuO_x clusters (inset), c) aggregates of highly-dispersed CuO_x in the 5CuNa catalyst on the surface of SiO_2 substrate, d) larger aggregates of CuO_x in the 10CuNa catalyst, e) STEM-EDS elemental mapping for the 5CuNa catalyst (scale bar is 200 nm, red = Cu, green = Si and blue = Na) and f) STEM-EDS elemental mapping of 10CuNa catalyst (scale bar is 200 nm). (For interpretation of the references to colour in this figure legend, the reader is referred to the web version of this article.)

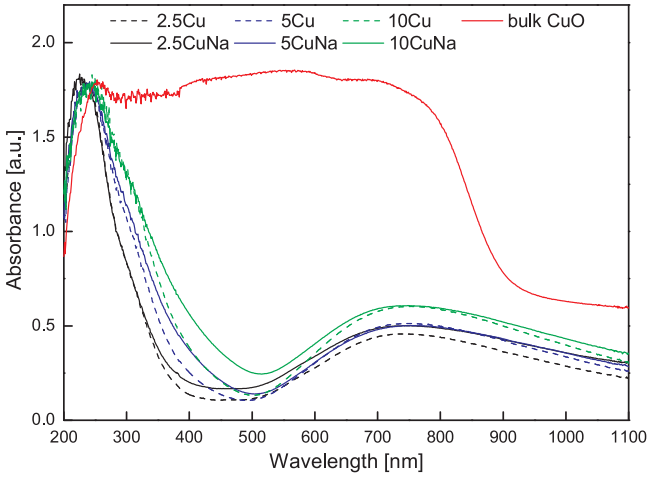

Fig. 4. The UV/VIS spectra of sodium unmodified and modified catalysts compared to bulk copper oxide.

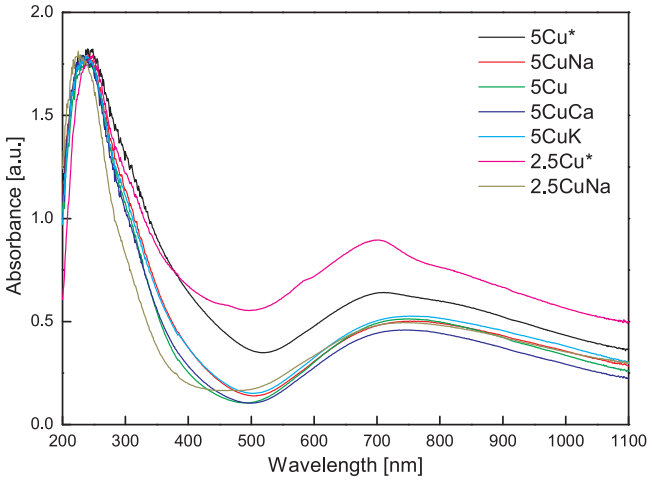

Fig. 5. The UV/Vis DR spectra of 2.5Cu, 2.5CuNa, 5Cu, 5CuNa, 5CuK and 5CuCa catalysts exhibiting identical thermal history, compared to the once calcined 5Cu catalyst. Samples marked with an asterisk were calcined twice, equaling thermal history of alkali modified catalysts.

3.1.6. Acid site probing with pyridine DRIFTS

Acid sites are known to negatively affect selectivity for PO, as these strongly electrophilic surface sites can react with bridging oxygen in PO, resulting in its further oxidation, or surface blocking and deactivation via strong adsorption [7]. The results of pyridine DRIFTS measurements for the 2.5Cu, 5Cu and 10Cu catalysts before and after Na modification, as well as pure KIT-6 support are presented in Fig. 7. Absence of the peak at 1550 cm^{-1} indicates no Brønsted acid sites on the analyzed samples. Based on the intensity of the band at 1450 cm^{-1}, deposition of 2.5–10 wt. % copper negligibly changes the Lewis acidity of the catalysts in comparison to pure KIT-6 silica support. On the other hand, sodium modification decreases the amount of Lewis acid sites for 44 and 29% in the 5CuNa and 10CuNa catalysts, respectively. The decrease in Lewis acid site abundance is in line with the sodium content, i.e. 0.8 and 0.5 wt. % in 5CuNa and 10CuNa catalysts, respectively (see Table S1).

3.1.7. Basic site probing with temperature programmed desorption (TPD) of CO_2 and hyphenated CO_2-TPD-DRIFTS technique

Surface basicity in heterogeneous catalysis is strongly related to nucleophilic nature of oxygen species on the catalyst surface [31], which play a decisive role in oxidation catalysis in terms of activity and selectivity [32,33]. Abundance and strength of basic sites in the synthesized catalysts was analyzed using CO_2-TPD analysis, which revealed two separate clusters of peaks for all the catalysts (Fig. 8a): a low-temperature cluster related to weak basic sites (between 0 and 300 °C), and a high-temperature cluster (comprised of two peaks centred at 450 and 600 °C) connected to strongly basic sites. Both clusters are comprised of several elemental peaks, indicating heterogeneous nature of the catalysts and consequently distribution of basic site strengths.

The weak and strong basic sites are very similar in strength for the 5Cu and 10Cu samples (Table 1, red and magenta lines in Fig. 8a). The main difference lies in a higher abundance of strong basic sites in the 10Cu catalyst. Alkali modification significantly affects both the abundance and strength of basic sites in both 5Cu and 10Cu catalysts; however, the action differs depending on the dopant (Table 2).

In the range of weak basic sites, the most striking difference is in the appearance of a shoulder at approximately 150 °C, which is observable only after modification in 5CuNa, 5CuK and 10CuNa catalysts.

Deconvolution of CO_2-TPD profiles (Fig. 8b) showed that in case of Na and K modification, the low-temperature cluster consists of three distinct peaks, centred at 60, 94 and 155 °C. The last peak is very broad and absent in unmodified and Ca modified catalysts.

The nature of CO_2 binding to the catalyst surface was further analyzed by a hyphenated CO_2-TPD-DRIFTS technique, showing difference spectra (Fig. 8c). Increase in band intensity in difference spectra indicates lower abundance (desorbed) species, whereas decreased intensity indicates formed species. The samples were pre-treated and saturated with CO_2 as described in Section 2.2.7. DRIFT spectra were recorded at temperatures determined by the positions of deconvoluted CO_2-TPD peaks (Fig. S2) in order to discriminate changes related to individual CO_2 desorption peaks.

Fig. 8c shows that up to 94 °C (first two CO_2 desorption peaks, black and red lines), mostly surface bound water and hydroxyls are removed (based on the bands at 1630 and 3100-3650 cm^{-1}). A significant amount of CO_2 is also desorbed in these two steps, as evident by the sharp band at 2339 cm^{-1}. The low desorption temperature and position of the absorption band close to the one of gas phase CO_2 (2350 cm^{-1}) are in line with the minimal electron back donation to the antibonding orbital of CO_2, confirming the electrostatic character of CO_2 desorbed below 94 °C [34]. Also, weak bands at 1320 and 1601 cm^{-1} indicate desorption of small amounts of formate species bound to copper, which are formed through reaction of adsorbed CO_2 and surface hydroxyl groups. The loss of band intensity at 1453 cm^{-1} indicates formation of surface monodentate carbonates in very small amounts already at 60 °C.

Between 94 and 250 °C (third CO_2 desorption peak centred at 150 °C) changes are more abundant, which is in line with broadness of the third CO_2 TPD peak (Fig. 8b). A small amount of water and physisorbed CO_2 are desorbed (based on the increase of band intensity at 1631 and 2339 cm^{-1}). The rise in band intensity at 1453 cm^{-1} indicates the decomposition of surface monodentate carbonates as well as carbonyl species (bands at 1890 and 2040 cm^{-1}). Considering that no carbon monoxide was detected during CO_2-TPD analysis, decomposition and desorption of carbonyl species is accompanied with extraction of an oxygen atom resulting in the reduction of CuO_x species. This is in line with the observed colour change of the 5CuNa sample during the CO_2-TPD analysis from light blue to dark brown, suggesting presence of reduced (metallic copper) species.

Substantial restructuring of the surface adsorbed CO_2 and oxygen in the CuO_x (and not reaction between CO_2 and H_2O and/or OH, based on very small changes in their bands) is also observed between 94 and 250 °C. Based on the decreased intensity of bands at 1105, 1250, 1350 and 1470 cm^{-1}, formation of carbonates and reduction of CuO_x to Cu_2O took place. Similar bands were observed by Chen et al. [34] during CO_2 chemisorption on Cu_2O.

Increasing the temperature from 250 to 690 °C (covering the high-temperature CO_2 desorption cluster, blue line in Fig. 8c) causes a substantial desorption of CO_2 (2339 cm^{-1}), water and hydroxyls (1630 and

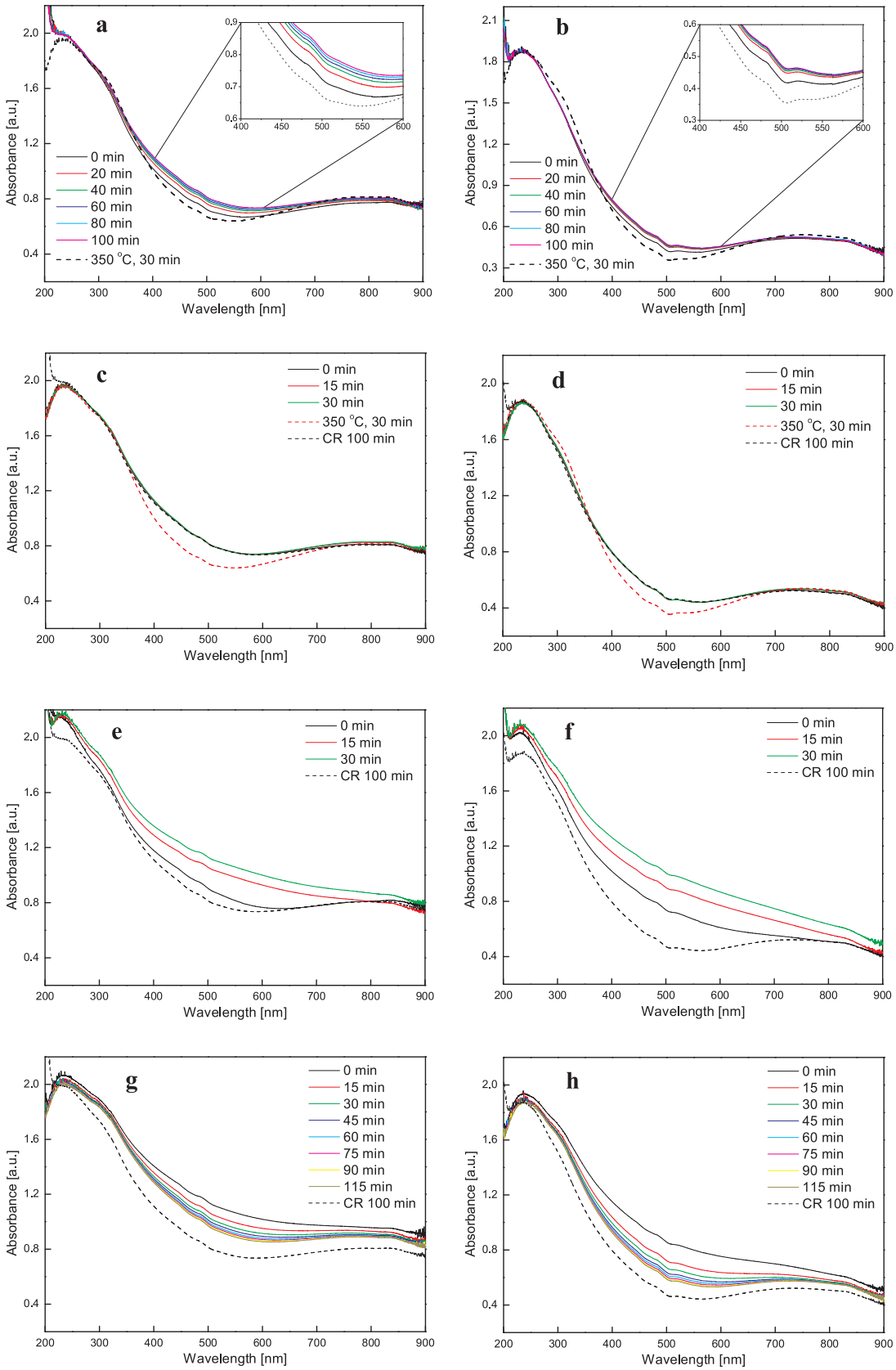

Fig. 6. The UV/VIS DR spectra of 5Cu (a, c, e and g) and 5CuNa (b, d, f and h) samples taken at specific time intervals during the catalytic propylene oxidation reaction (a,b), in an oxidative atmosphere after the reaction (c,d), in a reductive atmosphere of pure propylene (e,f), and in an oxidative atmosphere after reduction in propylene (g,h). In the legend, the spectrum "350 °C, 30 min" stands for spectrum measured after catalyst pre-treatment in O_2/He flow, while the spectrum "CR 100 min" stands for spectrum measured after 100 min of the propylene oxidation reaction.

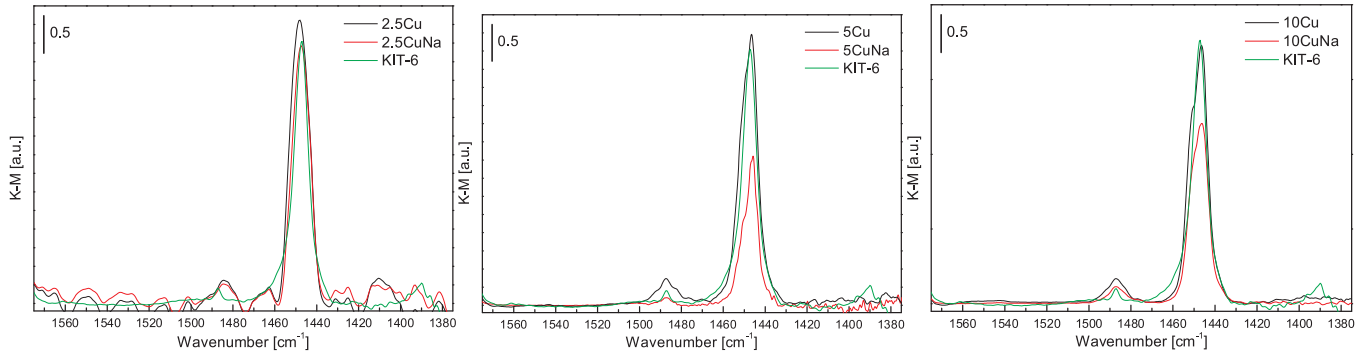

Fig. 7. DRIFT pyridine adsorption spectra of 2.5Cu, 5Cu and 10Cu catalysts before and after Na modification, as well as of bare KIT-6 SiO_2 support.

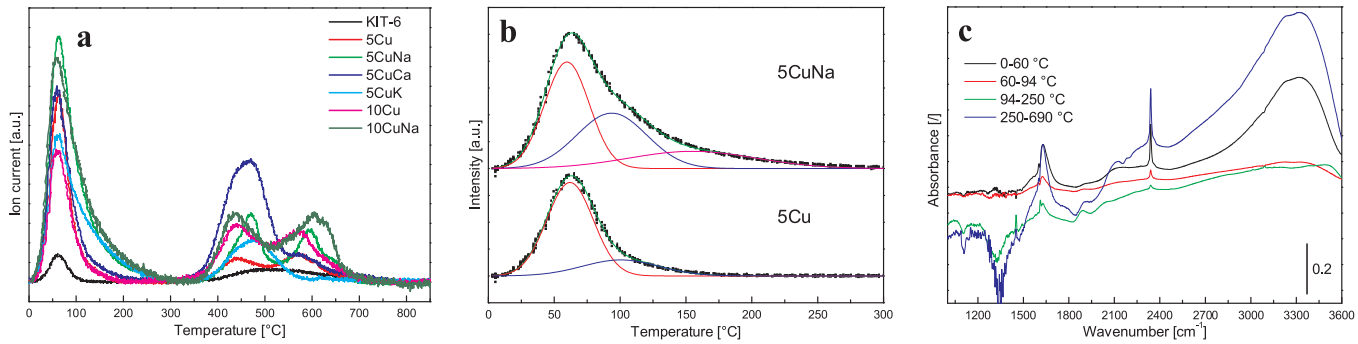

Fig. 8. The CO_2-TPD spectra of 5Cu and 10Cu catalysts prior to and after Na, Ca and K modification (a), deconvolution of the low-temperature CO_2 TPD peak for 5CuNa and 5Cu catalysts (b), and DRIFTS difference spectra measured at characteristic temperature intervals (Fig. S2) over 5CuNa catalyst during CO_2-TPD examination (c).

Table 2
Quantity of desorbed CO_2 for different catalysts.

Sample	Quantity of desorbed CO_2 (μmol × g_{cat}^{-1})		
	Low T cluster	High T cluster	Peak at 155 °C
KIT-6	6.5	12.5	0
5CuNa	65	32.5	13
5Cu	30	20	0
5CuCa	37.5	52.5	0
5CuK	50	17.5	16
10CuNa	75	55	21
10Cu	30	45	0

between 2500-3600 cm^{-1}) and elimination of carbonyl groups (1890 and 2130 cm^{-1}). Also, a decomposition of monodentate carbonate (1452 cm^{-1}) takes place, as well as formation of carbonates from adsorbed CO_2 with simultaneous reduction of CuO_x to Cu_2O.

To briefly summarize, with alkali modification, the nucleophilic character of the oxygen in CuO_x species is reduced. Modulation of the Cu-O bond strength is likely connected to close proximity of the electrophilic Na^+ to the [Cu-O-Cu] moiety, which attracts the partial negative charge of the oxygen atom (Scheme 1, Pathway 1) [18]. This results in the formation of new basic sites of intermediate strength. Oxygen in modified CuO_x appears to be more strongly bound, enabling the formation of loosely bound surface carbonate species, not present in unmodified catalysts.

3.1.8. *Operando* Cu K-edge XANES analysis

Operando Cu K-edge XANES analysis was used to determine the valence states and local symmetries of Cu cations in the 5Cu, 5CuNa and 5CuCa catalysts in the as prepared state, at 350 °C in the O_2/He atmosphere and during catalytic propylene oxidation (Fig. 9).

A shift of Cu K-edge energy of about 4 eV is observed between Cu^+ and Cu^{2+} compounds [36–39]. The characteristic pre-edge resonance or shoulder attributed to the Cu(1*s*-4*p*) transitions can be very effective in the identification of Cu^+ and Cu^{2+} species. In the crystalline Cu_2O, where monovalent Cu^+ is coordinated to four oxygen atoms, a well-defined absorption feature from the 1*s*-4*p* transition occurs at 8982.0 eV [37,38]. In the reference Cu_2O nanoclusters (Cu^+-containing MOR-type zeolite (Fig. 9) [35]), the 1*s*-4*p* transition occurs at 8983.4 eV. In case of Cu^{2+} compounds the 1*s*-4*p* transition appears as pre-edge shoulder in the energy range from 8985 eV to 8989 eV, the energy position and intensity of the shoulder depend on Cu^{2+} cation local symmetry. In the crystalline CuO the shoulder is at 8985.0 eV, while in the case of the reference sample, CuO nanoclusters dispersed in a zeolite, (Fig. 9.) the shoulder is at 8986.3 eV [35,37–39].

The energy position of Cu K-edge and pre-edge shoulder in 5Cu, 5CuNa and 5CuCa catalysts (at RT and 350 °C in He/O_2 atmosphere) matches with the reference sample containing Cu^{2+} oxide nanoclusters dispersed on a zeolite. Based on these references and LCF (linear combination fit) analysis of the 5Cu, 5CuNa and 5CuCa catalysts (at 350 °C in O_2/He atmosphere) all copper is present as Cu^{2+} and the majority (~90%) is subnanometer Cu^{2+} clusters. Only ~10% is present as nanocrystalline CuO (Fig. S4). This is in agreement with TEM-EDX and UV–vis analyses which identified polydisperse $[Cu\text{-}O\text{-}Cu]_x$ moieties as a predominant CuO_x phase, in coexistence with CuO nanocrystallites. The LCF analysis of XANES spectra showed that in the 5CuNa catalyst no sodium cuprate phase (which contains Cu^{3+}) is formed in O_2/He or C_3H_6/O_2/He atmosphere at 350 °C (Figs. S4 and S5).

The Cu K-edge XANES spectra measured during propylene oxidation reaction (Fig. 9.) clearly reveal a substantial reduction of Cu^{2+} to Cu^+ in all tested catalysts. The spectra exhibit a characteristic pre-edge resonance at 8982.7 eV that can be ascribed to the 1*s*-4*p* transition in Cu^+ cations in Cu_2O nanoclusters. The intensity of the resonance is proportional to the relative amount of Cu^+ cations in the sample and increases with prolonged TOS. After 300 min of propylene oxidation reaction, the amount of Cu^+ reaches different values for the tested

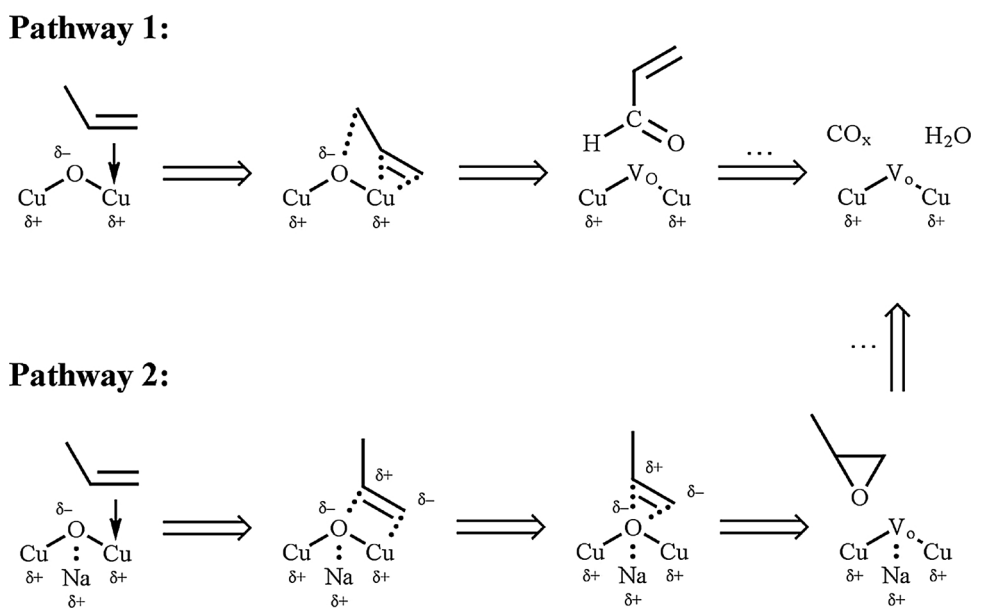

Scheme 1. Reaction pathways of propylene oxidation over CuO_x/SiO_2 catalyst with and without alkali modification.

catalysts: 57(± 5), 68(± 5) and 52(± 5) % for 5Cu, 5CuNa and 5CuCa, respectively (Fig. 10). Also, the dynamics of reaching a quasi-steady oxidation state are very different: the 5Cu catalyst stabilizes (within the quantification error) after 50 min of reaction. This time is prolonged to 100 min for the 5CuCa, whereas the 5CuNa still approaches the quasi-steady state after 300 min.

3.2. Catalytic propylene oxidation reaction

Results of the catalytic propylene oxidation reaction are presented in Figs. 11 and S7. Tests with pure or Na promoted KIT-6 SiO_2 support resulted in no propylene conversion during the 6 h test at 350 °C showing presence of CuO_x as prerequisite for any catalytic conversion.

Over the non-promoted catalysts, the reaction products are CO_2, CO, water, acrolein and trace amounts of other oxygenates (acetone, propanal, propanol, …). However, the latter present less than 5% of the C containing products and are not considered in the discussion. The selectivity over non-modified catalysts for individual reaction products does not change when copper loading is increased from 2.5 to 10 wt. % (Fig. 11b–d).

Low catalytic activity of the 2.5Cu and especially 1Cu catalysts (less than 2.5 and 1% initial propylene conversion, respectively) is likely related to the low amount of CuO_x phase. The 10Cu catalyst enabled highest (25%) initial propylene conversion. Regardless of the copper

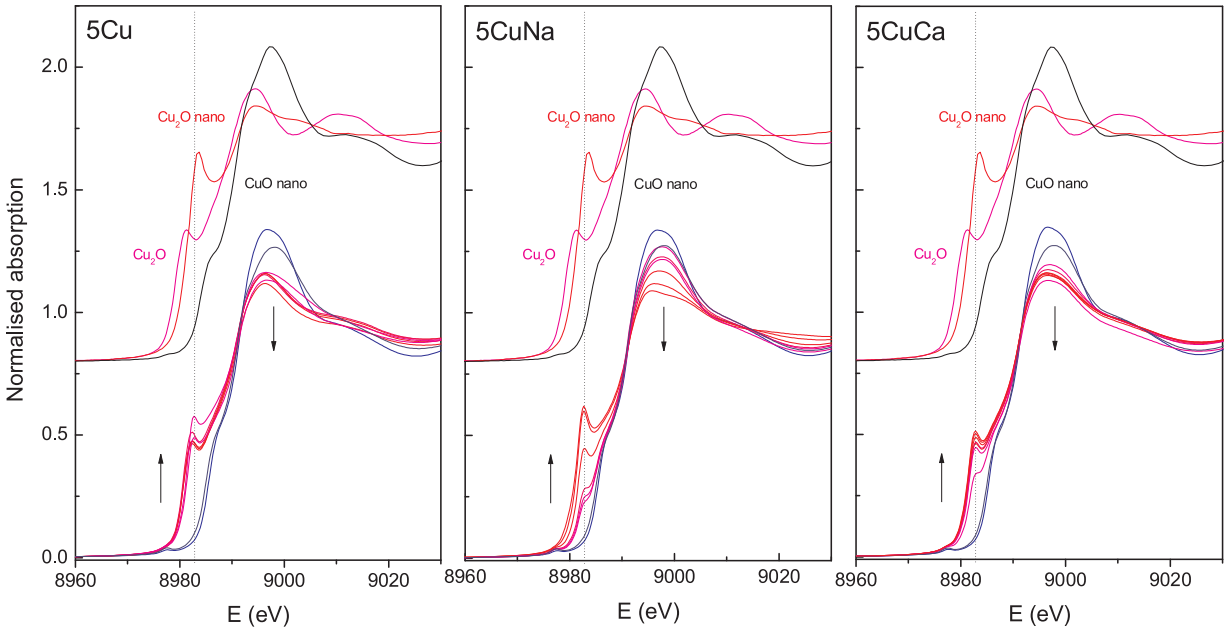

Fig. 9. Normalized Cu K-edge XANES spectra of 5Cu, 5CuNa and 5CuCa catalysts, measured *in-situ* before and during catalytic propylene oxidation reaction. The blue line represents the catalyst measured at RT in O_2/He atmosphere, black line the catalyst in O_2/He atmosphere at 350 °C. Temporal evolution of the catalyst during the propylene oxidation reaction is shown in magenta/red lines with vertical arrows highlighting gradually increasing Cu^+ and decreasing Cu^{2+} contribution. Spectra of reference Cu^+ and Cu^{2+} compounds (crystalline Cu_2O, nanoclusters Cu_2O [35] and CuO nanoparticles) are plotted for comparison. A vertical dashed line is plotted at the peak of the Cu 1s-4p pre-edge absorption feature (8982.7 eV) in the catalysts during the propylene oxidation reaction. (For interpretation of the references to colour in this figure legend, the reader is referred to the web version of this article.)

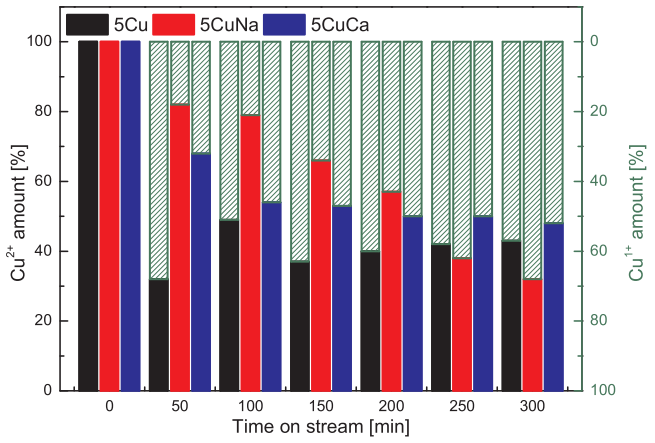

Fig. 10. Fractions of Cu^{2+} and Cu^{+} oxidation states in the 5Cu, 5CuNa and 5CuCa catalysts during the propylene oxidation reaction. The bars at t = 0 min refer to catalyst samples in O_2/He atmosphere at 350 °C.

content, strong deactivation is observed over all unmodified catalysts: they lost more than 60% of initial activity during the 17 h of propylene oxidation reaction (Fig. 11a). In the same time frame, over the 5Cu catalyst, acrolein selectivity increases from 50 to 70%, CO_x selectivity remains between 25–30 % and selectivity for other oxygenates decreased. Sintering of CuO_x phase during the course of reaction (confirmed by *operando* UV/Vis analysis) appears beneficial for acrolein formation which is favoured over bulk-like CuO. Furthermore, oxygen species of CuO_x, regardless of their structure (mononuclear Cu^{2+}-O and $[Cu\text{-}O\text{-}Cu]_n$ as well as bulk-like CuO) exhibit sufficient nucleophilic character to execute the attack on the allylic hydrogen of propylene and thus favour acrolein formation (Scheme 1, Pathway 1).

Based on the results of catalytic runs and *operando* XANES analysis we can conclude that a substantial fraction of Cu^{2+} is transformed to Cu^{+} during the propylene oxidation reaction (52–68 %, depending on the modifying atom). Also, the dynamics of reaching the quasi steady oxidation state differ strongly. However, none of these factors can be solely correlated to PO selectivity. We conclude that the kinetics of oxygen abstraction and replenishment are substantially different, revealing a modified chemistry of the nucleophilic oxygen species present in 5CuNa and 5CuK catalyst, in contrast to the others (5Cu and 5CuCa).

Modification of 5Cu catalysts with sodium and potassium greatly minimized catalyst deactivation (Fig. 11a): minimal deactivation is observed during 17 h TOS for the 5CuNa catalyst, whereas catalytic activity of 5CuK and 2.5CuNa stabilizes after 10 h following the initial decrease of about 25%. Post reaction elemental analysis of catalyst samples showed between 0 and 4 wt. % of carbon deposited during 17 h of reaction (Table S1). For the most promising catalysts investigated, these values are very low (up to 1.6 wt. %), which excludes catalyst fouling by polymerization of reaction intermediates and accumulation of carbonaceous deposits as a primary reason for deactivation.

After Na and K addition, a notable (~10%) propylene oxide selectivity was also observed (Fig. 11b), which increased with prolonging TOS. Having in mind progressive growth of $[Cu\text{-}O\text{-}Cu]_n$ clusters observed by *operando* UV/Vis analysis (Fig. 6b), it is reasonable to assume that Na and K modified oligomeric $[Cu\text{-}O\text{-}Cu]_n$ species (and not mononuclear Cu^{2+} sites) act as active sites responsible for PO formation. Na modification of the 10Cu catalyst exhibited a negligible

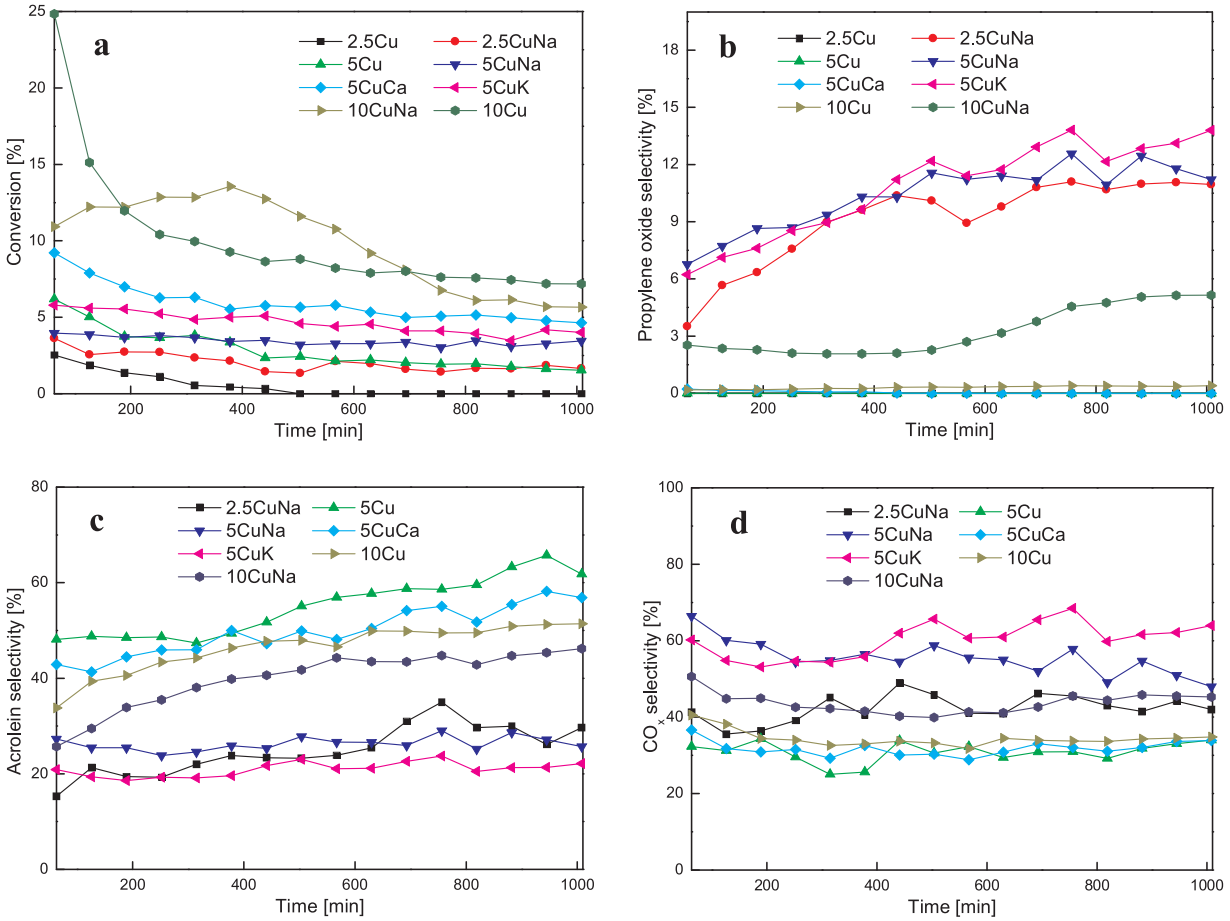

Fig. 11. a) Propylene conversion, b) PO selectivity, c) acrolein selectivity and d) CO_2 selectivity as a function of TOS for promoted and unpromoted 2.5Cu, 5Cu and 10Cu catalysts. The lines depicting the PO selectivity of 2.5Cu and 5Cu catalysts in Fig. b) are at 0% along with 10Cu and 5CuCa.

influence on the shift to PO selectivity (5%, Fig. 11b). This catalyst contains the largest fraction of bulk-like CuO (TEM and UV/Vis analyses, Figs. 3d, f and Fig. 4), which confirms the role of alkali modified bulk-like CuO_x in the propylene epoxidation pathway as minor (it dominates in the acrolein formation pathway). This is consistent with less efficient electronic modification of oxygen species in bulk CuO_x achieved by alkali doping (one alkali cation modulates nucleophilicity of 2–4 adjacent oxygen atoms, depending on the crystalline plane of CuO where it resides, instead of one or two oxygen atoms in $[Cu\text{-}O\text{-}Cu]_n$ oligomers) as well as the suggested requirement for spatial active site isolation in the selective oxidation reactions [40,41], as well as very localized alkali action. The PO weight time yield values obtained lie between 39 and 80 $g_{PO}/kg_{cat} \times h$ (Table S2) for all tested catalysts. The numbers are comparable to values obtained by others over K doped CuO_x/SiO_2 (116 $g_{PO}/kg_{cat} \times h$) [19] and FeO_x/SiO_2 catalysts (47 $g_{PO}/kg_{cat} \times h$) [42].

The selectivity for acrolein is substantially lower (70 and 20% at 17 h TOS, and changes marginally during the whole experiment) when comparing modified 5CuK and 5CuNa catalysts to 5Cu sample. On the other hand, selectivity for CO_2 is notably higher after alkali modification (Fig. 11c) and does not correlate with the abundance of Lewis acid (Fig. 7), or strength or abundance of basic sites (Table 2). Additional propylene oxidation experiment with 5Cu and 5CuNa catalysts and co-fed PO into the gas feed stream showed that over both catalysts, PO is further oxidized and CO_x is the main product (Fig. S6). The unmodified 5Cu catalyst converts approximately 90% of co-fed PO, whereas over the 5CuNa catalyst, only 75% of PO is further oxidized. Consequently, both chemical aspects of the catalyst design, as well as engineering aspects and reaction conditions (reactor design, temperature, pressure and reactant concentration) need attention in order to achieve the goal of appropriate PO selectivity as described by Khatib and Oyama [4].

Two independent reaction pathways occur during propylene oxidation over alkali modified CuO_x/SiO_2 catalysts, as shown in Scheme 1 and Fig. S6.

Pathway 1: Propylene adsorption takes place via the C=C bond to the copper adatom. The oxygen in [Cu-O-Cu] moieties initiates a nucleophilic attack on the allylic hydrogen. The allylic hydrogen is stripped and the terminal carbon is oxidized, producing acrolein. Upon re-adsorption of the primary product, acrolein, on the catalyst's surface, subsequent oxidation occurs, producing CO_x and H_2O.

In Pathway 2, propylene adsorption takes place via the C=C bond to the copper adatom. The nucleophilic character of the oxygen in [Cu-O-Cu] moieties is lessened by the adjacent alkali metal, making its nucleophilic attack on the allylic hydrogen less effective. With the polarization of the double bond, the central carbon can bind the oxygen atom and form an oxametallacycle. The stabilization effect of the Na (or K) modification allows the metal-carbon bond to break [11], which leads to physisorbed propylene oxide, which ultimately desorbs as PO. Subsequent oxidation of PO to CO_x also occurs, but to a lesser extent compared to a non-modified CuO_x/SiO_2 catalyst (Fig. S6).

He et al. [29] used kinetic analysis to identify two independent and parallel reaction pathways over Cs modified 5% CuO_x/SiO_2 catalysts producing PO and acrolein, with PO readily being isomerized further to allyl alcohol. A very likely reason that only trace amounts of allyl and isopropyl alcohol were observed during our tests is that a much higher temperature (350 vs. 250 °C) was used in the present study, which substantially accelerated also the reaction rates towards final oxidation products (CO and CO_2).

By progressively increasing the Na content in the 5Cu catalyst (Table S1, Fig. 12), different fraction of oxygen species and their nucleophilic character can be modified. This is manifested as higher PO selectivity (Fig. 12b), while a reverse trend is observed in acrolein selectivity (Fig. 12c). The PO selectivity increase, achieved when changing the Cu:Na ratio from 1:0.43 to 1:0.6, is relatively small (11 vs. 13%). This indicates that the Cu:Na molar ratio of 1:0.43 (5CuNa catalyst) used for the modification is very close to the optimum.

With calcium modification of the 5Cu catalyst, a dramatic increase in the initial catalytic activity is observed (9 and 6.5% propylene conversion for 5CuCa and 5Cu catalysts, respectively) with trace (below 0.5%) PO selectivity (Fig. 11a and b). Acrolein and CO_x selectivities remain very similar to the unmodified 5Cu catalyst.

Alkali and earth alkali modification of the CuO_x/SiO_2 catalysts produces a diametrally different effect on PO selectivity. The PO selectivity vs. dopant electronegativity plot (Fig. S7) based on the data obtained in this study and other works [19,29], indicates that PO selectivity decreases with increasing electronegativity of the alkali metals ($Cs < Rb \approx K < Na < Li < Ca < Mg$). The Na^+ and K^+ represent localized positive charges which, adjacent to the [Cu-O-Cu] entities (TEM elemental mapping, Fig. 3e and f), attract electrons from the oxygen thus decreasing its nucleophilic strength. As a result, the catalytic action of oxygen changes from oxidative attack on the allylic hydrogen to oxygen insertion into the C=C bond of propylene.

When earth alkali metals are used as dopants, PO selectivity is negligible. We are speculating that as the electronegativity (the tendency of an atom to attract electrons) and valency of the dopant increase (as in the case of Ca^{2+} modified sample), the attraction becomes limited not only to the negative charge of adjacent oxygen in CuO_x, but also to other anionic species, such as hydroxyl groups. A similar phenomenon has been observed before when conducting catalytic reactions in the liquid-phase, with hydroxyl groups forming a progressively denser Helmholtz layer around alkali and earth alkali cations [43]. As a result of charge compensated by hydroxyl groups, the doping efficiency is decreased and negligible after earth alkali modification.

Total oxidation always occurs to a certain extent during the propylene oxidation reaction, which produces CO_x and water, which can further decompose to form surface hydroxyl groups. Abundance and binding strength of hydroxyl groups to the catalyst surface was analyzed using H_2O-TPD-MS technique (Fig. 13). It can be seen that a 5 wt. % Cu addition to KIT-6 silica causes a twofold increase in the density of water and hydroxyls. Their number is decreased by 15–25 % after Na and K modification, respectively. There is a general similarity between the K and Na modified 5Cu and 10Cu catalysts as well as some similarity between the unmodified 5Cu and 10Cu catalysts and the one modified with calcium. However, the largest abundance and strength of hydroxyl binding to the catalyst surface (based on the position of the high-temperature desorption peak) is observed after modification with calcium. The high temperature peaks confirm pure KIT-6 silica dehydroxylation upon heating to 900 °C. The amount of desorbed water becomes much more prominent after copper addition. The results of H_2O-TPD analysis are in line with the proposed role of hydroxyl groups negating the positive charge of alkali and earth alkali cations, thus opposing their effect.

4. Conclusions

The synthesized CuO_x/SiO_2 catalysts contain finely dispersed [Cu-O-Cu] moieties with different degrees of polymerization, as well as CuO_x clusters of 2–6 nm in size. These form larger aggregates as Cu content increases from 2.5 to 10 wt. %. According to the *operando* XANES analysis, the working state of the alkali modified and non-modified catalysts is predominantly Cu^+, between 52–68 %, depending on the modifying atom. Sintering of the CuO_x phase during the course of the reaction promotes acrolein formation, which appears favored over bulk-like CuO_x. Oxygen species contained in mononuclear Cu^{2+}-O and $[Cu\text{-}O\text{-}Cu]_n$ as well as bulk-like CuO all exhibit sufficient nucleophilic character to execute the attack on the allylic hydrogen and thus circumvent PO formation. Consequently, a shift of selectivity towards PO is possible only with alkali modification of the oxygen species contained in CuO_x. The time resolved dynamics of the Cu^+ fraction depends strongly on the modifying atom and indicates different kinetics of oxygen abstraction and replenishment. This suggests modified chemistry of the nucleophilic oxygen species, present in 5CuNa and 5CuK

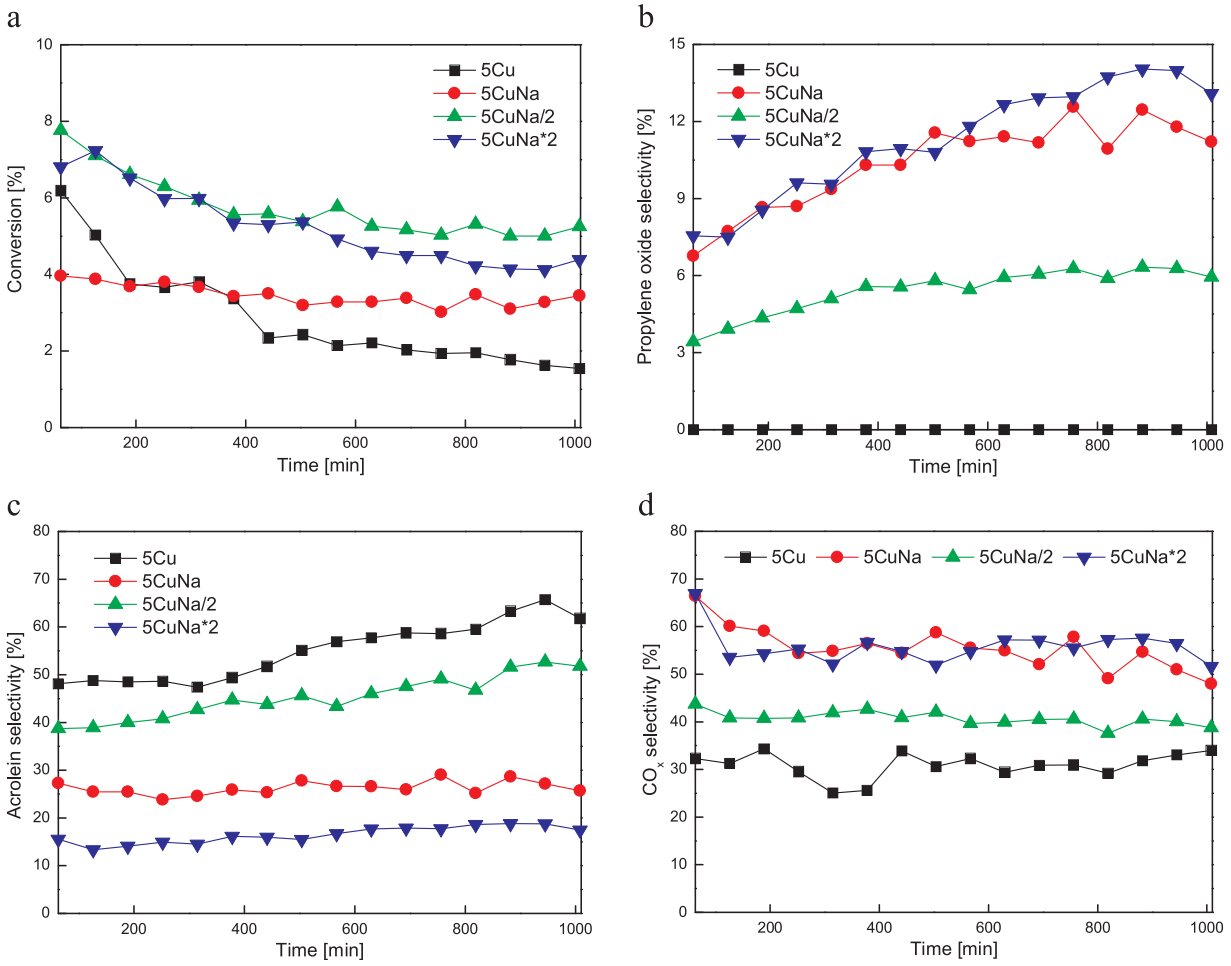

Fig. 12. a) Propylene conversion, b) PO selectivity, c) acrolein selectivity, and d) CO_2 selectivity as a function of TOS for 5Cu catalysts promoted with different amounts of Na.

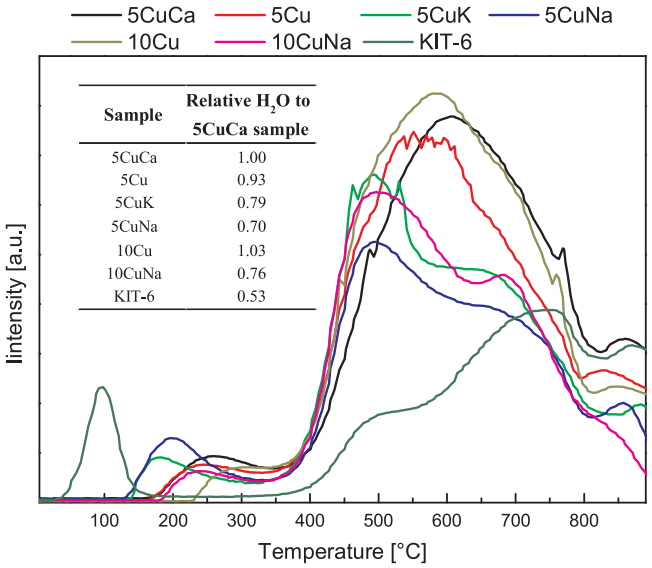

Sample	Relative H_2O to 5CuCa sample
5CuCa	1.00
5Cu	0.93
5CuK	0.79
5CuNa	0.70
10Cu	1.03
10CuNa	0.76
KIT-6	0.53

Fig. 13. The MS spectra recorded during H_2O-TPD experiments over alkali and earth alkali mofified 5Cu and 10Cu catalysts. Samples (100 mg) were positioned inside a U-shaped quartz reactor and pre-treated in a flow 5% O_2/He at 350 °C for 30 min. After pre-treatment, they were cooled to 100 °C. The samples were heated to 900 °C at 5 °C/min and H_2O desorption was monitored by a mass spectrometer (Pfeiffer Vacuum, model ThermoStar™ GSD320) following the characteristic m/z = 18 fragment.

catalysts in contrast to others (5Cu and 5CuCa). As a result, Cu^+ is not crucial for PO formation, but instead less nucleophilic oxygen and the geometry of the active site (PO formation is favored on oligomeric [Cu-O-Cu]$_x$ moieties and not mononuclear Cu^{2+}-O species). TEM-EDS analyses show that alkali metal cations are finely dispersed over the support and closely associated with the CuO_x phase. The modification with Na^+ and K^+ decreases the nucleophilic strength of CuO_x oxygen, by attracting its electrons, making its attack on the allylic hydrogen of propylene less effective. It also decreases [Cu-O-Cu] sintering. These changes manifest themselves as greatly improved catalytic stability during the propylene oxidation reaction, accompanied by a notable shift in selectivity from acrolein towards propylene oxide. Alkali modification generates basic sites of intermediate strength, confirmed by a CO_2-TPD-DRIFTS analysis, which are not present in non-modified CuO_x/SiO_2 catalysts. This supports altered chemistry/reactivity of surface oxygen species after alkali modification. Subsequent oxidation of formed PO and acrolein to CO_x also occurs, but to a lesser extent compared to a non modified catalyst, due to lowered oxygen reactivity.

With increasing electronegativity and use of two valent dopants, a different effect is achieved: higher catalytic activity and stability, compared to non modified catalysts, but no change in selectivity. The decrease of the nucleophilic character of O species in CuO_x by Ca^{2+} is negated by the charge compensation with strongly adsorbed adjacent hydroxyl groups; hence, earth alkali doping efficiency on PO selectivity is inefficient.

Acknowledgements

JT, PD and AP acknowledge financial support through Research program P2-0150 and research grant Z2-5463 provided by the Slovenian Research Agency (ARRS). MS acknowledges financial support through Research program P2-0091. IA acknowledges the financial support from the Slovenian Research Agency (research core funding No. P1-0112), Access to synchrotron radiation facilities (XAFS beamline, project 20170045) of ELETTRA is acknowledged, and JT acknowledges the support by the project CALIPSOplus under the Grant Agreement 730872 from the EU Framework Programme for Research and Innovation HORIZON 2020 for the XAS experiment at Elettra. We thank Giuliana Aquilanti, Simone Pollastri, Mateusz Czyzycki and Ricardo Grisonich from XAFS beamline for the assistance during experiment and expert advice on beamline operation. The authors kindly acknowledge Dr. Maxim Zabilskiy for the reference spectrum of nanocrystalline CuO and access to the European Synchrotron Radiation Facility (Dutch-Belgian beamline BM26 A, pr. CH-5057).

Appendix A. Supplementary data

Supplementary material related to this article can be found, in the online version, at doi:https://doi.org/10.1016/j.apcatb.2018.05.092.

References

[1] D. Torres, N. Lopez, F. Illas, R.M. Lambert, Low-basicity oxygen atoms: a key in the search for propylene epoxidation catalysts, Angew. Chemie - Int. Ed. 46 (2007) 2055–2058, http://dx.doi.org/10.1002/anie.200603803.
[2] The Dow Chemical Company, Propylene Oxide, (2013) http://msdssearch.dow.com/PublishedLiteratureDOWCOM/dh_096d/0901b8038096db15.pdf?filepath=productsafety/pdfs/noreg/233-00305.pdf&fromPage=GetDoc.
[3] V. Russo, R. Tesser, E. Santacesaria, M. Di Serio, Chemical and technical aspects of propene oxide production via hydrogen peroxide (HPPO process), Ind. Eng. Chem. Res. 52 (2013) 1168–1178, http://dx.doi.org/10.1021/ie3023862.
[4] S.J. Khatib, S.T. Oyama, Direct oxidation of propylene to propylene oxide with molecular oxygen: a review, Catal. Rev. 57 (2015) 306–344, http://dx.doi.org/10.1080/01614940.2015.1041849.
[5] C. Qi, T. Akita, M. Okumura, M. Haruta, Epoxidation of propylene over gold catalysts supported on non-porous silica, Appl. Catal. A Gen. 218 (2001) 81–89, http://dx.doi.org/10.1016/S0926-860X(01)00621-4.
[6] S. Lee, L.M. Molina, M.J. López, J.A. Alonso, B. Hammer, B. Lee, S. Seifert, R.E. Winans, J.W. Elam, M.J. Pellin, S. Vajda, Selective propene epoxidation on immobilized Au6-10 clusters: the effect of hydrogen and water on activity and selectivity, Angew. Chemie Int. Ed. 48 (2009) 1467–1471, http://dx.doi.org/10.1002/anie.200804154.
[7] G. Mul, Stability and selectivity of Au/ TiO2 and Au/ TiO2/SiO2 catalysts in propene epoxidation: an in situ FT-IR study, J. Catal. 201 (2001) 128–137, http://dx.doi.org/10.1006/jcat.2001.3239.
[8] J.R. Monnier, The direct epoxidation of higher olefins using molecular oxygen, Appl. Catal. A Gen. 221 (2001) 73–91, http://dx.doi.org/10.1016/S0926-860X(01)00799-2.
[9] J. Lu, J.J. Bravo-Suárez, M. Haruta, S.T. Oyama, Direct propylene epoxidation over modified Ag/CaCO3 catalysts, Appl. Catal. A Gen. 302 (2006) 283–295, http://dx.doi.org/10.1016/j.apcata.2006.01.023.
[10] M. Mavrikakis, D.J. Doren, M.A. Barteau, Density functional theory calculations for simple oxametallacycles: trends across the periodic table, J. Phys. Chem. B. 102 (1998) 394–399, http://dx.doi.org/10.1021/jp971450p.
[11] A. Kokalj, P. Gava, S. de Gironcoli, S. Baroni, What determines the catalyst's selectivity in the ethylene epoxidation reaction, J. Catal. 254 (2008) 304–309, http://dx.doi.org/10.1016/j.jcat.2008.01.008.
[12] X. Yang, S. Kattel, K. Xiong, K. Mudiyanselage, S. Rykov, S.D. Senanayake, J.A. Rodriguez, P. Liu, D.J. Stacchiola, J.G. Chen, Direct epoxidation of propylene over stabilized Cu + + surface sites on titanium-modified Cu + 2O, Angew. Chemie - Int. Ed. 54 (2015) 11946–11951, http://dx.doi.org/10.1002/anie.201504538.
[13] W. Su, S. Wang, P. Ying, Z. Feng, C. Li, A molecular insight into propylene epoxidation on Cu/SiO2 catalysts using O2 as oxidant, J. Catal. 268 (2009) 165–174, http://dx.doi.org/10.1016/j.jcat.2009.09.017.
[14] O. Vaughan, G. Kyriakou, N. Macleod, M. Tikhov, R. Lambert, Copper as a selective catalyst for the epoxidation of propene, J. Catal. 236 (2005) 401–404, http://dx.doi.org/10.1016/j.jcat.2005.10.019.
[15] M.T. Greiner, T.E. Jones, B.E. Johnson, T.C.R. Rocha, Z.J. Wang, M. Armbrüster, M. Willinger, A. Knop-Gericke, R. Schlögl, The oxidation of copper catalysts during ethylene epoxidation, Phys. Chem. Chem. Phys. 17 (2015) 25073–25089, http://dx.doi.org/10.1039/C5CP03722K.
[16] J.R. Monnier, G.W. Hartley, Comparison of Cu and Ag catalysts for epoxidation of Higher olefins, J. Catal. 203 (2001) 253–256, http://dx.doi.org/10.1006/jcat.2001.3336.
[17] A. Marimuthu, J. Zhang, S. Linic, Tuning selectivity in propylene epoxidation by plasmon mediated photo-switching of Cu oxidation state, Science 339 (2013) 1590–1593, http://dx.doi.org/10.1126/science.1231631.
[18] Q. Hua, T. Cao, X.-K. Gu, J. Lu, Z. Jiang, X. Pan, L. Luo, W.-X. Li, W. Huang, Crystal-plane-controlled selectivity of Cu 2 o catalysts in propylene oxidation with molecular oxygen, Angew. Chemie Int. Ed. 53 (2014) 4856–4861, http://dx.doi.org/10.1002/anie.201402374.
[19] Y. Wang, H. Chu, W. Zhu, Q. Zhang, Copper-based efficient catalysts for propylene epoxidation by molecular oxygen, Catal. Today 131 (2008) 496–504, http://dx.doi.org/10.1016/j.cattod.2007.10.022.
[20] W. Yao, Y.L. Guo, X.H. Liu, Y. Guo, Y.Q. Wang, Y.S. Wang, Z.G. Zhang, G.Z. Lu, Epoxidation of propylene by molecular oxygen Over the Ag–Y2O3–K2O/α-Al2O3 catalyst, Catal. Lett. 119 (2007) 185–190, http://dx.doi.org/10.1007/s10562-007-9220-8.
[21] A. Held, J. Kowalska-Kuś, K. Nowińska, K. Góra-Marek, Potassium-modified silica-supported vanadium oxide catalysts applied for propene epoxidation, J. Catal. 347 (2017) 21–35, http://dx.doi.org/10.1016/j.jcat.2016.12.001.
[22] J. García-Aguilar, D. Cazorla-Amorós, Á. Berenguer-Murcia, K- and Ca-promoted ferrosilicates for the gas-phase epoxidation of propylene with O 2, Appl. Catal. A Gen. 538 (2017) 139–147, http://dx.doi.org/10.1016/j.apcata.2017.03.031.
[23] T. Kim, F. Kleitz, B. Paul, R. Ryoo, MCM-48-like large mesoporous silicas with tailored Pore structure: facile synthesis domain in a ternary triblock copolymer – butanol – water system, J. Am. Chem. Soc. 127 (2005) 7601–7610, http://dx.doi.org/10.1021/ja042601m.
[24] M. Meng, Y. Liu, Z. Sun, L. Zhang, X. Wang, Synthesis of highly-dispersed CuO-CeO2 catalyst through a chemisorption-hydrolysis route for CO preferential oxidation in H 2-rich stream, Int. J. Hydrogen Energy 37 (2012) 14133–14142, http://dx.doi.org/10.1016/j.ijhydene.2012.07.075.
[25] J. Wang, Y. Li, Z. Zhang, Z. Hao, Mesoporous KIT-6 silica–polydimethylsiloxane (PDMS) mixed matrix membranes for gas separation, J. Mater. Chem. A 3 (2015) 8650–8658, http://dx.doi.org/10.1039/C4TA07127A.
[26] S. Lomate, A. Sultana, T. Fujitani, Effect of SiO 2 support properties on the performance of Cu–SiO 2 catalysts for the hydrogenation of levulinic acid to gamma valerolactone using formic acid as a hydrogen source, Catal. Sci. Technol. 7 (2017) 3073–3083, http://dx.doi.org/10.1039/C7CY00902J.
[27] P. Kuśtrowski, L. Chmielarz, R. Dziembaj, P. Cool, E.F. Vansant, Dehydrogenation of ethylbenzene with nitrous oxide in the presence of mesoporous silica materials modified with transition metal oxides, J. Phys. Chem. A 109 (2005) 330–336, http://dx.doi.org/10.1021/jp0455881.
[28] H. Praliaud, S. Mikhailenko, Z. Chajar, M. Primet, Surface and bulk properties of Cu–ZSM-5 and Cu/Al2O3 solids during redox treatments. Correlation with the selective reduction of nitric oxide by hydrocarbons, Appl. Catal. B: Environ. 16 (1998) 359–374, http://dx.doi.org/10.1016/S0926-3373(97)00093-3.
[29] J. He, Q. Zhai, Q. Zhang, W. Deng, Y. Wang, Active site and reaction mechanism for the epoxidation of propylene by oxygen over CuOx/SiO2 catalysts with and without Cs + + modification, J. Catal. 299 (2013) 53–66, http://dx.doi.org/10.1016/j.jcat.2012.11.032.
[30] F. Boccuzzi, S. Coluccia, G. Martra, N. Ravasio, Cu/SiO2 and Cu/SiO2–TiO2 catalysts, J. Catal. 184 (1999) 316–326, http://dx.doi.org/10.1006/jcat.1999.2428.
[31] G. Busca, Acid and basic catalysts: fundamentals, Heterog. Catal. Mater. Elsevier, 2014, pp. 57–101, http://dx.doi.org/10.1016/B978-0-444-59524-9.00005-5.
[32] F. Polo-Garzon, S.-Z. Yang, V. Fung, G.S. Foo, E.E. Bickel, M.F. Chisholm, D. Jiang, Z. Wu, Controlling reaction selectivity through the surface termination of perovskite catalysts, Angew. Chemie Int. Ed. 56 (2017) 9820–9824, http://dx.doi.org/10.1002/anie.201704656.
[33] N. Mizuno, Modern Heterogeneous Oxidation Catalysis, Wiley-VCH Verlag GmbH & Co, KGaA, Weinheim, Germany, 2009, http://dx.doi.org/10.1002/9783527627547.
[34] S. Chen, T. Cao, Y. Gao, D. Li, F. Xiong, W. Huang, Probing surface structures of CeO 2, TiO 2, and Cu 2 O nanocrystals with CO and CO 2 chemisorption, J. Phys. Chem. C 120 (2016) 21472–21485, http://dx.doi.org/10.1021/acs.jpcc.6b06158.
[35] E.M.C. Alayon, M. Nachtegaal, A. Bodi, M. Ranocchiari, J.A. van Bokhoven, Bis(μ-oxo) versus mono(μ-oxo)dicopper cores in a zeolite for converting methane to methanol: an in situ XAS and DFT investigation, Phys. Chem. Chem. Phys. 17 (2015) 7681–7693, http://dx.doi.org/10.1039/C4CP03226H.
[36] F.W. Lytle, R.B. Greegor, A.J. Panson, Discussion of x-ray-absorption near-edge structure: application to Cu in the high-Tc superconductors La1.8Sr0.2CuO4 and YBa2Cu3O7, Phys. Rev. B. 37 (1988) 1550–1562, http://dx.doi.org/10.1103/PhysRevB.37.1550.
[37] A. Manceau, A. Matynia, The nature of Cu bonding to natural organic matter, Geochim. Cosmochim. Acta. 74 (2010) 2556–2580, http://dx.doi.org/10.1016/j.gca.2010.01.027.
[38] C. Maurizio, F. D'Acapito, M. Benfatto, S. Mobilio, E. Cattaruzza, F. Gonella, Local coordination geometry around Cu and Cu ions in silicate glasses: an X-ray absorption near edge structure investigation, Eur. Phys. J. B. 14 (2000) 211–216, http://dx.doi.org/10.1007/s100510050122.
[39] O. Pliekhova, I. Arčon, O. Pliekhov, N.N. Tušar, U.L. Štangar, Cu and Zr surface sites in the photocatalytic activity of TiO2nanoparticles, Environ. Sci. Pollut. Res. 24 (2017) 12571–12581, http://dx.doi.org/10.1007/s11356-016-7685-y.
[40] R.K. Grasselli, Fundamental principles of selective heterogeneous oxidation catalysis, Top. Catal. 21 (2002) 79–88, http://dx.doi.org/10.1023/A:1020556131984.
[41] C.A. Carrero, R. Schloegl, I.E. Wachs, R. Schomaecker, Critical literature review of the kinetics for the oxidative dehydrogenation of propane over Well-defined supported vanadium oxide catalysts, ACS Catal. 4 (2014) 3357–3380, http://dx.doi.org/10.1021/cs5003417.
[42] J. García-Aguilar, I. Miguel-García, J. Juan-Juan, I. Such-Basáñez, E. San Fabián, D. Cazorla-Amorós, Á. Berenguer-Murcia, One step-synthesis of highly dispersed iron species into silica for propylene epoxidation with dioxygen, J. Catal. 338 (2016) 154–167, http://dx.doi.org/10.1016/j.jcat.2016.03.004.
[43] A. Pintar, M. Šetinc, J. Levec, Hardness and Salt effects on catalytic hydrogenation of aqueous nitrate solutions, J. Catal. 174 (1998) 72–87, http://dx.doi.org/10.1006/jcat.1997.1960.